PHYSICAL REVIEW B **95**, 041410(R) (2017)

Magnetoresistance and quantum oscillations of an electrostatically tuned semimetal-to-metal transition in ultrathin WTe_2

Valla Fatemi,[1] Quinn D. Gibson,[2] Kenji Watanabe,[3] Takashi Taniguchi,[3] Robert J. Cava,[2] and Pablo Jarillo-Herrero[1]
[1]*Department of Physics, Massachusetts Institute of Technology, Cambridge, Massachusetts 02139, USA*
[2]*Department of Chemistry, Princeton University, Princeton, New Jersey 08544, USA*
[3]*Advanced Materials Laboratory, National Institute for Materials Science, 1-1 Namiki, Tsukuba 305-0044, Japan*
(Received 15 November 2016; revised manuscript received 27 December 2016; published 30 January 2017)

We report on electronic transport measurements of electrostatically gated nanodevices of the semimetal WTe_2. High mobility metallic behavior is achieved in the 2D limit by encapsulating thin flakes in an inert atmosphere. At low temperatures, we find that a large magnetoresistance can be turned on and off by electrostatically doping the system between a semimetallic state and an electron-only metallic state, respectively. We confirm the nature of the two regimes by analyzing the magnetoresistance and Hall effect with a two-carrier model, as well as by analysis of Shubnikov-de Haas oscillations, both of which indicate depletion of hole carriers via the electrostatic gate. This confirms that semiclassical transport of two oppositely charged carriers accurately describes the exceptional magnetoresistance observed in this material. Finally, we also find that the magnetoresistance power law is subquadratic and density independent, suggesting new physics specifically in the semimetallic regime.

DOI: 10.1103/PhysRevB.95.041410

Semimetals, electronic systems with partially populated bands of both positive and negative curvature, have been sources of novel physics since at least 1930, with the discovery of Shubnikov-de Haas (SdH) oscillations in bismuth [1,2]. The semimetal graphite, when thinned down to the electronically two-dimensional (2D) limit, displays remarkable physics that continues to be explored [3,4]. Even more recently, three-dimensional (3D) bulk semimetals have had a resurgence of interest due to recently discovered experimental and theoretical behaviors, including unusually large magnetoresistances [5,6] and new topological electronic states known as Dirac and Weyl semimetals [7,8].

The compound WTe_2 bridges both of these phenomena: Experimentally it showcases exceptionally large, quadratic magnetoresistance in magnetic fields up to 60 T [9], and theoretically it is predicted to be a Weyl semimetal in 3D [10] and near a quantum spin Hall state in 2D [11]. The observed magnetoresistance in bulk samples has been proposed to be the result of near-compensated electron and hole carriers, described by a semiclassical two carrier model [5,12,13]. However, a number of questions have been raised regarding the mechanisms at play. First, quantum oscillations revealed multiple Fermi pockets as well as imperfect compensation [14–16], suggesting other effects may play a role. Moreover, the small Fermi energy and orbital helicity of the Fermi surface suggest that the band structure and scattering mechanisms, respectively, are liable to change under application of a magnetic field [17–19]. To elucidate the origins of the magnetoresistance, a natural experiment would be to study the effect of changing the carrier density of a thin sample *in situ*, which recent transport studies have attempted with varying results [20–22]. A major difficulty at the ultrathin limit is that sample quality degrades significantly as the thickness is reduced: Oxidation induces insulating behavior below six layers thick, rendering phenomena related to the high quality bulk crystals inaccessible in the 2D limit [21,23,24].

In this Rapid Communication, we investigate exfoliated WTe_2 devices that are fabricated in a glove box under inert atmosphere in order to minimize degradation [25]. Doing so enables creation of high quality nanodevices that display the intrinsic physics of the material [26]. At low temperatures, we use an electrostatic gate to dope the system from a semimetallic regime to a single-carrier regime. During this crossover we observe an evolution of the magnetoresistance and Hall effect that is qualitatively well captured by a semiclassical two-carrier model. We additionally observe that the exponent of the magnetoresistance power law is subquadratic and gate independent within the semimetallic regime. Finally, the semimetal-to-metal transition is further confirmed by analysis of SdH oscillations, which give insight to the low-energy band structure.

To fabricate the devices, WTe_2 is exfoliated in an argon atmosphere (<1 ppm oxygen) and then encapsulated between layers of hexagonal boron nitride (h-BN) with a polymer pick-up and transfer technique [27]. For the device discussed in the main text, we also include few-layer graphene (FLG) between the WTe_2 and the bottom h-BN layer as an electronic contact. This FLG layer has a natural lateral gap between two independent sheets, which the WTe_2 spans. Finally, we contact the FLG with evaporated Cr-Au via the edge-contact technique [28] and then etch the device into a Hall bar geometry with a reactive ion etch. The FLG serves as an intermediary conductor between the evaporated electrodes and the WTe_2 while also maintaining a good van der Waals seal with the encapsulating h-BN [29]. The device sits on a doped silicon wafer with 285 nm of thermal SiO_2, which serve as the back-gate electrode and dielectric, respectively. All electronic transport measurements are conducted in a four-probe configuration. An optical micrograph and a schematic cross section of the device are shown in Figs. 1(a) and 1(b). Here we report on the behavior of a three-layer thick device (sample A, thickness confirmed by AFM and Raman spectroscopy [21]), and in the Supplemental Material we show data on additional devices [30].

The first indication that inert atmosphere fabrication maintains crystal integrity is the temperature dependence of the

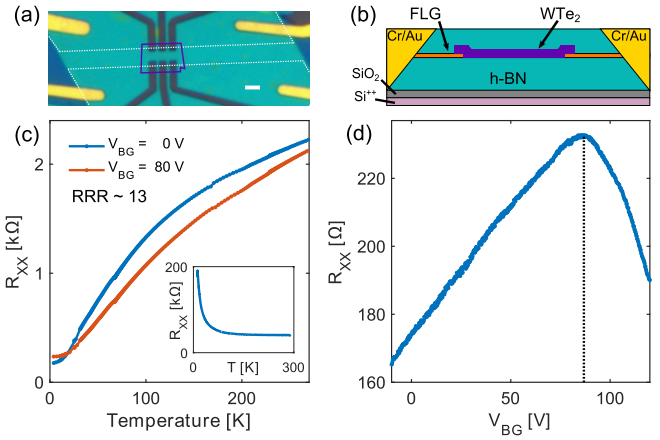

FIG. 1. (a) Optical image of a completed device. The edges of the original FLG flakes are indicated by dashed white line, and the original boundary of the WTe_2 flake is outlined in purple. The dark regions are where the stack was fully etched to the SiO_2 substrate. Solid white scale bar is 2 microns long. (b) Cross-sectional schematic of the device structure, with all components labeled. (c) Temperature dependence of device A at two representative gate voltages. The average RRR for all gate voltages is 13. Inset: Temperature dependence of a similar-thickness WTe_2 device fabricated in air and without encapsulation. (d) Gate dependence of R_{xx} at $B = 0$ T and $T = 4$ K. The vertical dashed line at $V_{BG} = 87$ indicating the resistance maximum.

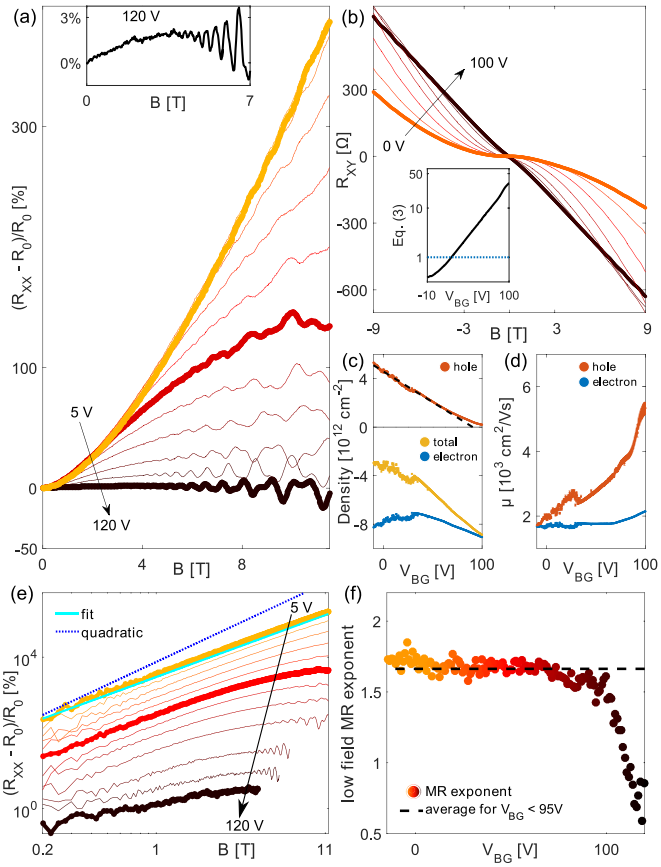

FIG. 2. (a) MR as a function of magnetic field for a range of V_{BG} at $T = 30$ mK. Inset: a zoom-in of the data at $V_{BG} = 120$ V. (b) R_{xy} as a function of magnetic field for a range of V_{BG} at $T = 300$ mK, displaying a transition from nonlinear to linear Hall effect [31]. Inset: Extracted saturation parameter [Eq. (3)] as a function of gate voltage (black) at $B = 10$ T. The blue dotted line is unity. (c) Individual carrier densities and the total carrier density, including charge sign, from the semiclassical model fit. Black dashed line is an extrapolation of the hole density from the slope at lower gate voltages. (d) Mobilities from the model fit. Error bars in (c) and (d) represent 95% confidence intervals of the fit. (e) Same data as (a) in log-log format with each curve offset vertically for clarity. The blue dotted line is a quadratic power law, whereas the cyan line is a power law fit to the data at $V_{BG} = 10$ V. (f) The fitted exponent of the MR power law for $B \in [0.4, 1.5]T$ as a function of gate voltage. The limits were chosen to avoid the high relative noise at low fields ($B < 0.2$ T) and onset of saturation at high field. Dot color corresponds to gate voltage in accordance with (a) and (e). Dot size is larger than the 95% confidence interval of the fit. The black dashed line indicates the mean exponent for $V_{BG} < 95$ V.

resistance, shown in Fig. 1(c). We observe metallic behavior with a residual resistivity ratio (RRR) of 13. In contrast, nonencapsulated devices fabricated in air display insulating behavior [inset of Fig. 1(c)]. In fact, in the literature a RRR of 13 is only achieved for samples greater than 33 nm thick [21]. Applying a bias V_{BG} to the electrostatic gate, we capacitively modulate the carrier density in the sample, finding that the low-temperature resistivity increases linearly with V_{BG} until ~87 V, beyond which the resistivity drops sharply [see Fig. 1(d)] [31]. The noted metallic temperature dependence with RRR of order 10 is observed for all gate voltages, with two representative gate voltages shown in Fig. 1(c).

We then measure both the longitudinal (R_{xx}) and transverse (R_{xy}) resistances as a function of magnetic field and gate voltage in order to investigate the magnetoresistance behavior at different total carrier densities. Both measurements are shown in Figs. 2(a) and 2(b) for a range of gate voltages, where in Fig. 2(a) we plot the magnetoresistance ratio (MR), defined as $(R_{xx}(B) - R_{xx}(0))/R_{xx}(0)$ [31]. The MR shows a clear transition from strong, superlinear behavior near zero gate voltage (~400% increase at 11.5T) to suppressed MR (<3%) at the highest gate voltage [inset of Fig. 2(a)]. During the crossover at intermediate gate voltages, we find that R_{xx} saturates at large B, as expected for a noncompensated semimetal [32,33]. Importantly, we observe that this crossover coincides with the Hall effect transitioning from nonlinear to linear magnetic field dependence, indicating a transition from two carrier types to a single carrier type.

To investigate this behavior in more detail, we employ the semiclassical two-carrier model, which gives the following equations for the longitudinal and transverse resistivity of a semimetal:

$$\rho_{xx} = \frac{1}{e}\frac{n\mu_n + p\mu_p + (n\mu_p + p\mu_n)\mu_n\mu_p B^2}{(n\mu_n + p\mu_p)^2 + (p-n)^2\mu_n^2\mu_p^2 B^2} \quad (1)$$

$$\rho_{xy} = \frac{1}{e}\frac{(p\mu_p^2 - n\mu_n^2)B + (p-n)\mu_n^2\mu_p^2 B^3}{(n\mu_n + p\mu_p)^2 + (p-n)^2\mu_n^2\mu_p^2 B^2}, \quad (2)$$

which include the electron charge e and four free parameters: the density (n, p) and mobility ($\mu_{n,p}$) of each carrier type, where n and p refer to electronlike and holelike carriers,

respectively. We fit $R_{xx}(B)$ and $R_{xy}(B)$ simultaneously to extract all four quantities at each gate voltage. (Here we constrain the electron density based on the SdH analysis presented below, but the important qualitative behavior doesn't require this. See Supplemental Material for details [30].) The fit parameters are plotted as a function of V_{BG} in Figs. 2(c) and 2(d). Most notably, we find that the hole density decreases monotonically to nearly zero at $V_{BG} \sim 100$ V, consistent with our earlier, qualitative interpretation of the data.

We highlight now a particular aspect of the semiclassical model regarding the onset of saturation (or absence thereof). The condition for onset of significant saturation in the MR is given by the ratio of the two terms in the denominator of Eq. (1):

$$\frac{(p-n)^2\mu_n^2\mu_p^2B^2}{(n\mu_n+p\mu_p)^2} \sim 1, \tag{3}$$

which is plotted in the inset to Fig. 2(b) for $B = 10$ T. This condition is satisfied for $V_{BG} > 22$ V, around which gate voltage we see the onset of saturation in the MR. The ratio is greater than 10 for $V_{BG} > 70$ V for which gate voltages we observe near complete saturation at high magnetic field. When seemingly unsaturating MR is observed in a semimetal, Eq. (3) can set a bound for the degree of noncompensation. For example, Ali *et al.* [5] measure effectively no saturation in bulk WTe_2 in fields up to 60 T. From this and the mobility (which sets the magnitude of the MR), one may estimate an upper bound for the relative carrier density difference $|\frac{n-p}{n+p}| \lesssim 0.3\%$, which is an order of magnitude smaller than that estimated from SdH measurements of the bulk Fermi surface [14,18]. This suggests that other factors may be involved in avoiding saturation at the highest fields for 3D samples [20]. A possible avenue would be to investigate the role of mobility anisotropies, known to be important in bismuth [34]. Nonetheless, for the range of magnetic fields studied here, our analysis confirms that the large MR observed in WTe_2 is rooted in the nearly compensated electron and hole densities.

Upon closer examination of our data, we find that the MR is actually subquadratic [35]. We can see this clearly by looking at the data in log-log format, as shown in Fig. 2(e). An explicit fit of the power law gives an exponent near 1.6, which is consistent for sample A in two different cooldowns as well as for additional devices presented in the Supplemental Material [30]. The exponent is stable for nearly all gate voltages for all devices, except above $V_{BG} \sim 100$ V for sample A, beyond which the exponent drops rapidly [Fig. 2(f)]. This dropoff coincides with the indications of depletion of the holes, reinforcing that the MR can be understood as that of a standard semimetal with a correction to the exponent.

The origin of the correction to the exponent is as yet unclear. Many studies on bulk WTe_2 have noted a large, quadratic MR [5,14,16,18,21,22,36], but some that explicitly fit the power law also find subquadratic exponents [20,37]. While we observe a similar deviation, our sample is in the 2D limit, whereas the Fermi surface of bulk WTe_2 is 3D in character [14,18], suggesting that dimensionality is not a driving factor. Additionally, we find that the power law is density independent in the semimetallic regime, and almost no MR is observed in the electron-only regime. This suggests that the coexistence of electrons and holes is crucial. One might look to semimetallic Boltzmann transport models which predict that boundary effects can generate linear MR when the valley recombination length is comparable to the transport channel width [12,13], but this requires classically strong magnetic fields not present here ($\mu_{n,p}B \lesssim 3$ for this work). Interspecies drag effects may also play a role in magnetoresistance [38], but finite intervalley scattering should suppress such physics. The question of the unusual magnetoresistance poses an experimental and theoretical challenge for future investigation.

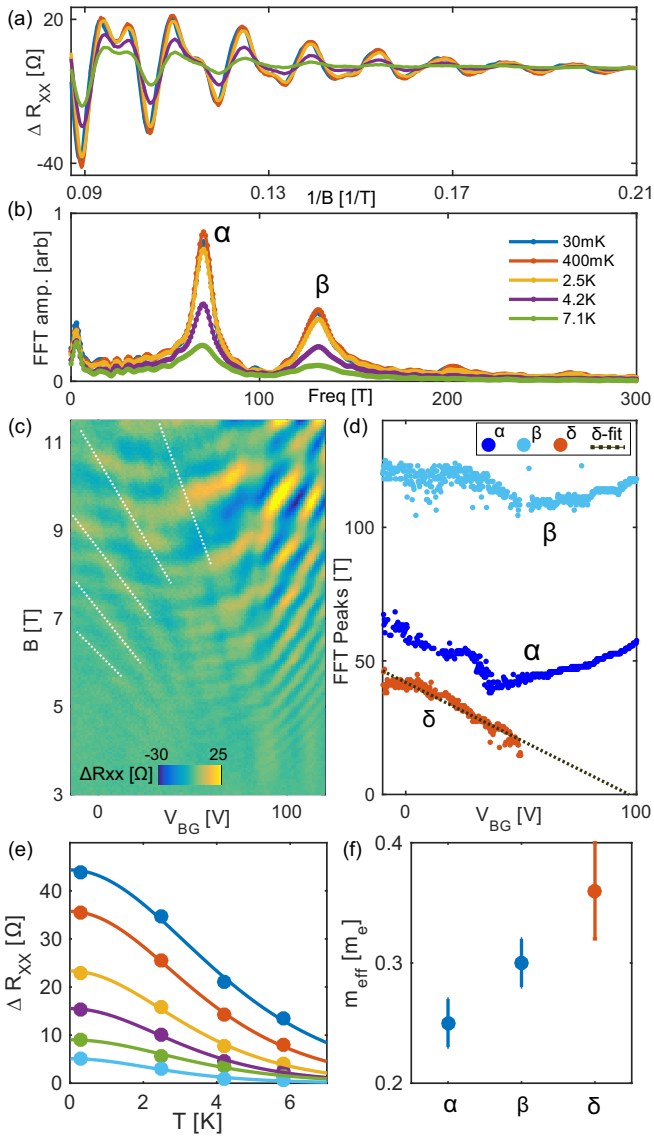

FIG. 3. (a) SdH oscillations in $\Delta R_{xx}(1/B)$ at different temperatures and (b) their fast Fourier transforms (FFTs) at $V_{BG} = 120$ V. (c) Gate and field dependence of ΔR_{xx} at $T = 30$ mK. White dotted lines guide the eye to the δ pocket oscillation. (d) FFT peak frequencies (dots) at each gate voltage and extrapolation of the δ frequency to zero (dotted line). (e) Temperature dependence of ΔR_{xx} maxima associated with the α pocket at $V_{BG} = 120$ V. (f) Effective mass of each pocket, from fits such as in (e) (see Supplemental Material for more details [30]).

We now turn to analysis of the quantum oscillations. In Fig. 3(a) we show representative measurements of $\Delta R_{xx}(1/B)$, the resistivity after subtracting a smooth quadratic background above 2 T, in the electron-only regime ($V_{BG} = 120$ V). At this gate voltage, two oscillations are clearly visible, confirmed by the two peaks visible in the Fourier transform of the data in Fig. 3(b), which we label α and β. In Fig. 3(c) we show a map of ΔR_{xx} with respect to both B and V_{BG}. A third, holelike dispersing oscillation is additionally visible for lower gate voltages (highlighted by dotted white lines), which we label δ. This is made clearer by fast Fourier transform (FFT) analysis, as shown in Fig. 3(d) where the three observed peak frequencies are tracked as a function of gate voltage [30]. The α and β frequencies disperse weakly with gate voltage in a very similar manner as the electron carrier density from the semiclassical analysis. The nonmonotonic gate dependence of the electron bands is likely the result of strong electric field effects, which can be explored in future devices employing a dual-gate geometry [11,39]. The third oscillation frequency, δ, decreases monotonically with increasing gate voltage, which we can extrapolate to zero frequency (full depletion) at roughly $V_{BG} = 90$ V. This depletion voltage agrees with what is found for the positive charge carriers in the semiclassical analysis, so we ascribe the δ pocket to a valence band. Curiously, this depletion also coincides with a peak in the amplitude of the SdH oscillations of the α and β pockets [see Fig. 3(c)], suggesting that scattering between the electron and hole valleys is important.

We also conduct temperature dependence of the SdH oscillations. Fitting the Lifshitz-Kosevich formula to the temperature dependence of resistance oscillation maxima allows for extraction of the effective mass. In multiband systems care must be taken to extract the oscillation amplitude of an individual frequency, which can be done by an appropriate FFT analysis (see Supplemental Material for more details [30]). An example fit for the α pocket oscillation is shown in Fig. 3(e), giving $m_\alpha/m_e = 0.25 \pm 0.02$, where m_e is the bare electron mass. Similar analysis for the other bands give $m_\beta/m_e = 0.30 \pm 0.02$ and $m_\delta/m_e = 0.36 \pm 0.04$ [see Fig. 3(f)] [30,40]. These values are somewhat smaller than those reported for bulk crystals, which range from 0.3 to 1 m_e [14,36]. The electron effective masses are in good agreement with theory for the monolayer, while the hole mass is again smaller than that prediction by about a factor of two [41]. We note that explicit predictions for few-layer WTe_2 have not yet been made.

In summary, we investigated electronic transport in encapsulated, ultrathin WTe_2. We find that a strong, intrinsic MR can be turned off by electrostatically doping the sample from a semimetallic state to an electron-only regime. We confirm the basis of the two regimes by simultaneously analyzing the MR and the Hall effect with a two-carrier model as well as by analysis of Shubnikov-de Haas oscillations, both of which indicate depletion of holelike carriers in the suppressed-MR regime. These observations confirm that the MR in WTe_2 is qualitatively explained by semiclassical transport of a semimetal, with potentially new physics in a modified exponent to the MR power law.

This work was partly supported by the DOE, Basic Energy Sciences Office, Division of Materials Sciences and Engineering, under award DE-SC0006418 (sample fabrication and measurements) and partly through AFOSR Grant No. FA9550-16-1-0382 (data analysis), as well as the Gordon and Betty Moore Foundation's EPiQS Initiative through Grant No. GBMF4541 to P.J.H.. Device nanofabrication was partly supported by the Center for Excitonics, an Energy Frontier Research Center funded by the DOE, Basic Energy Sciences Office, under Award No. DE-SC0001088. Crystal growth at Princeton University was supported by the NSF MRSEC program Grant No. DMR-1005438. This work made use of the Materials Research Science and Engineering Center Shared Experimental Facilities supported by NSF under Award No. DMR-0819762. Sample fabrication was performed partly at the Harvard Center for Nanoscale Science supported by the NSF under Grant No. ECS-0335765. We thank E. Navarro-Moratalla, J. D. Sanchez-Yamagishi, and L. Bretheau for discussions and Sanfeng Wu for help with crystal exfoliation.

[1] L. Schubnikow and W. J. d. Haas, Proceedings of the Netherlands Royal Academy of Science **33**, 130 (1930).

[2] D. Shoenberg, *Magnetic Oscillations in Metals* (Cambridge University Press, Cambridge, UK, 2009).

[3] M. O. Goerbig, Rev. Mod. Phys. **83**, 1193 (2011).

[4] S. Das Sarma, S. Adam, E. H. Hwang, and E. Rossi, Rev. Mod. Phys. **83**, 407 (2011).

[5] M. N. Ali, J. Xiong, S. Flynn, J. Tao, Q. D. Gibson, L. M. Schoop, T. Liang, N. Haldolaarachchige, M. Hirschberger, N. P. Ong, and R. J. Cava, Nature (London) **514**, 205 (2014).

[6] C. Shekhar, A. K. Nayak, Y. Sun, M. Schmidt, M. Nicklas, I. Leermakers, U. Zeitler, Y. Skourski, J. Wosnitza, Z. Liu, Y. Chen, W. Schnelle, H. Borrmann, Y. Grin, C. Felser, and B. Yan, Nat. Phys. **11**, 645 (2015).

[7] O. Vafek and A. Vishwanath, Annu. Rev. Condens. Matt. Phys. **5**, 83 (2014).

[8] S.-Y. Xu, I. Belopolski, N. Alidoust, M. Neupane, G. Bian, C. Zhang, R. Sankar, G. Chang, Z. Yuan, C.-C. Lee, S.-M. Huang, H. Zheng, J. Ma, D. S. Sanchez, B. Wang, A. Bansil, F. Chou, P. P. Shibayev, H. Lin, S. Jia, and M. Z. Hasan, Science **349**, 613 (2015).

[9] M. N. Ali, L. Schoop, J. Xiong, S. Flynn, Q. Gibson, M. Hirschberger, N. P. Ong, and R. J. Cava, Europhys. Lett. **110**, 67002 (2015).

[10] A. A. Soluyanov, D. Gresch, Z. Wang, Q. Wu, M. Troyer, X. Dai, and B. A. Bernevig, Nature (London). **527**, 495 (2015).

[11] X. Qian, J. Liu, L. Fu, and J. Li, Science **346**, 1344 (2014).

[12] G. Babkin and V. Y. Kravchenko, JETP **33**, 378 (1971).

[13] P. S. Alekseev, A. P. Dmitriev, I. V. Gornyi, V. Y. Kachorovskii, B. N. Narozhny, M. Schütt, and M. Titov, Phys. Rev. Lett. **114**, 156601 (2015).

[14] Z. Zhu, X. Lin, J. Liu, B. Fauqué, Q. Tao, C. Yang, Y. Shi, and K. Behnia, Phys. Rev. Lett. **114**, 176601 (2015).

[15] I. Pletikosić, M. N. Ali, A. V. Fedorov, R. J. Cava, and T. Valla, Phys. Rev. Lett. **113**, 216601 (2014).

[16] Y. Wu, N. H. Jo, M. Ochi, L. Huang, D. Mou, S. L. Bud'ko, P. C. Canfield, N. Trivedi, R. Arita, and A. Kaminski, Phys. Rev. Lett. **115**, 166602 (2015).

[17] J. Jiang, F. Tang, X. C. Pan, H. M. Liu, X. H. Niu, Y. X. Wang, D. F. Xu, H. F. Yang, B. P. Xie, F. Q. Song, P. Dudin, T. K. Kim, M. Hoesch, P. K. Das, I. Vobornik, X. G. Wan, and D. L. Feng, Phys. Rev. Lett. **115**, 166601 (2015).

[18] D. Rhodes, S. Das, Q. R. Zhang, B. Zeng, N. R. Pradhan, N. Kikugawa, E. Manousakis, and L. Balicas, Phys. Rev. B **92**, 125152 (2015).

[19] P. K. Das, D. Di Sante, I. Vobornik, J. Fujii, T. Okuda, E. Bruyer, A. Gyenis, B. E. Feldman, J. Tao, R. Ciancio, G. Rossi, M. N. Ali, S. Picozzi, A. Yadzani, G. Panaccione, and R. J. Cava, Nat. Commun. **7**, 10847 (2016).

[20] Y. Wang, K. Wang, J. Reutt-Robey, J. Paglione, and M. S. Fuhrer, Phys. Rev. B **93**, 121108 (2016).

[21] L. Wang, I. Gutiérrez-Lezama, C. Barreteau, N. Ubrig, E. Giannini, and A. F. Morpurgo, Nat. Commun. **6**, 8892 (2015).

[22] Lin Wang, Ignacio Gutierrez-Lezama, Celine Barreteau, Dong-Keun Ki, Enrico Giannini, and Alberto F. Morpurgo, Phys. Rev. Lett. **117**, 176601 (2016).

[23] C.-H. Lee, E. C. Silva, L. Calderin, M. A. T. Nguyen, M. J. Hollander, B. Bersch, T. E. Mallouk, and J. A. Robinson, Sci. Rep. **5**, 10013 (2015).

[24] Fan Ye, Jaesung Lee, Jin Hu, Zhiqiang Mao, Jiang Wei, and Philip X.-L. Feng, Small **12**, 5802 (2016).

[25] Zaiyao Fei, Tauno Palomaki, Sanfeng Wu, Wenjin Zhao, Xinghan Cai, Bosong Sun, Paul Nguyen, Joseph Finney, Xiaodong Xu, and David H. Cobden, arXiv:1610.07924.

[26] A. W. Tsen, R. Hovden, D. Wang, Y. D. Kim, J. Okamoto, K. A. Spoth, Y. Liu, W. Lu, Y. Sun, J. C. Hone, L. F. Kourkoutis, P. Kim, and A. N. Pasupathy, Proc. Natl. Acad. Sci. USA **112**, 15054 (2015).

[27] C. R. Dean, A. F. Young, I. Meric, C. Lee, L. Wang, S. Sorgenfrei, K. Watanabe, T. Taniguchi, P. Kim, K. L. Shepard, and J. Hone, Nat. Nanotechnol. **5**, 722 (2010).

[28] L. Wang, I. Meric, P. Y. Huang, Q. Gao, Y. Gao, H. Tran, T. Taniguchi, K. Watanabe, L. M. Campos, D. A. Muller, J. Guo, P. Kim, J. Hone, K. L. Shepard, and C. R. Dean, Science **342**, 614 (2013).

[29] X. Cui, G.-H. Lee, Y. D. Kim, G. Arefe, P. Y. Huang, C.-H. Lee, D. A. Chenet, X. Zhang, L. Wang, F. Ye, F. Pizzocchero, B. S. Jessen, K. Watanabe, T. Taniguchi, D. A. Muller, T. Low, P. Kim, and J. Hone, Nat. Nanotechnol. **10**, 534 (2015).

[30] See Supplemental Material at http://link.aps.org/supplemental/10.1103/PhysRevB.95.041410 for (1) details of the two carrier analysis and fits, (2) investigation of the FLG-WTe2 contact resistance, (3) more information on the SdH oscillation analysis, and (4) additional data on other devices.

[31] Data in Fig. 1 are from initial measurements in a 4 K probe. Data and analysis in Figs. 2(b)–2(d) are from a second cooldown at 300 mK (more details in the Supplemental Material). All other data and analysis in the main text are from a third cooldown with a base temperature of 30 mK.

[32] X. Du, S.-W. Tsai, D. L. Maslov, and A. F. Hebard, Phys. Rev. Lett. **94**, 166601 (2005).

[33] P. B. Alers and R. T. Webber, Phys. Rev. **91**, 1060 (1953).

[34] A. Collaudin, B. Fauqué, Y. Fuseya, W. Kang, and K. Behnia, Phys. Rev. X **5**, 021022 (2015).

[35] While the nonparabolicity of the low-field MR may introduce a systematic error to the fits by the semiclassical MR equations, it does not change the qualitative behavior of the fit parameters nor our general conclusions—similar behavior is observed when fitting the Hall data with a constraint given only by the zero-field longitudinal resistance (see Supplemental Material for details [30]). Lacking a physical model for the modified power law, we choose not to artificially alter the two-carrier model for the fits.

[36] P. L. Cai, J. Hu, L. P. He, J. Pan, X. C. Hong, Z. Zhang, J. Zhang, J. Wei, Z. Q. Mao, and S. Y. Li, Phys. Rev. Lett. **115**, 057202 (2015).

[37] L. R. Thoutam, Y. L. Wang, Z. L. Xiao, S. Das, A. Luican-Mayer, R. Divan, G. W. Crabtree, and W. K. Kwok, Phys. Rev. Lett. **115**, 046602 (2015).

[38] B. N. Narozhny and A. Levchenko, Rev. Mod. Phys. **88**, 025003 (2016).

[39] T. Taychatanapat and P. Jarillo-Herrero, Phys. Rev. Lett. **105**, 166601 (2010).

[40] At least 20 different fits to the temperature dependence of resistance maxima at several gate voltages are averaged to obtain the mean effective mass.

[41] H. Y. Lv, W. J. Lu, D. F. Shao, Y. Liu, S. G. Tan, and Y. P. Sun, Europhys. Lett. **110**, 37004 (2015).